

**TEMPERATURE GRADIENTS RECORDED BY FLUID INCLUSIONS
AND HYDROTHERMAL ALTERATION AT THE MOUNT CHARLOTTE GOLD DEPOSIT,
KALGOORLIE, AUSTRALIA**

TERRENCE P. MERNAGH[§]

Geoscience Australia, GPO Box 378, Canberra, ACT 2601, Australia

CHRISTOPH A. HEINRICH

*Swiss Federal Institute of Technology, ETH Zürich, Isotope Geology and Mineral Resources,
ETH Zentrum, NO CH-8092 Zürich, Switzerland*

EDWARD J. MIKUCKI

2285 Coolgardie Street, Mundaring, WA 6073, Australia

ABSTRACT

The Mount Charlotte gold deposit, Kalgoorlie, Australia, comprises a series of steeply plunging orebodies in which a network of conjugate quartz veins are surrounded by sulfide-rich alteration haloes that host most of the gold. There are three mineralogically distinct types of alteration halo, which are systematically distributed on the orebody scale, with pyrite-rich haloes at the top and in the periphery of the deposit, and pyrrhotite-rich alteration at depth and in the center of the fluid-upflow zones. Fluid inclusions in the main-stage quartz from veins within each of the three alteration assemblages have been analyzed to determine possible thermal and chemical trends on the scale of the deposit. Fluid-inclusion assemblages associated with the shallow and more distal pyrite–muscovite alteration contain three-phase H₂O–CO₂ inclusions and coexisting liquid-rich, aqueous inclusions with less than 15 vol.% vapor. The lowest-temperature Fluid Inclusion Assemblages (FIAs) from this alteration assemblage homogenize between 210 and 245°C. FIAs in quartz veins in pyrite–pyrrhotite alteration contain two-phase H₂O–CO₂–CH₄ inclusions and liquid-rich, aqueous inclusions. The lowest-temperature FIAs in this assemblage homogenize between 240 and 275°C. Veins in pyrrhotite–albite alteration contain two-phase H₂O–CO₂–CH₄ inclusions and liquid-rich, aqueous inclusions, with the lowest-temperature FIAs homogenizing from 260 to 310°C. A late, secondary population of liquid-rich H₂O–CH₄ inclusions was also observed in veins associated with pyrite–muscovite and pyrrhotite–albite alteration. These inclusions homogenize between 239 and 286°C. Although the temperature ranges overlap, the fluid-inclusion data and alteration data consistently indicate a significant gradient in temperature between the base and the top of the deposit (up to 100°C / km) during vein stockwork formation and alteration at Mount Charlotte. In contrast, the chemical composition of the fluids in terms of H₂O : CO₂ : CH₄ : NaCl, as determined by microthermometry and Raman-microprobe analyses, do not vary in a systematic manner on the deposit scale, although the CH₄ : CO₂ ratio varied across a large range. These observations indicate that gold deposition at Mount Charlotte occurred by desulfidation of bisulfide complexes due to reaction with Fe-rich wallrocks to form pyrrhotite and pyrite, as previously suggested. These reactions are strongly temperature-dependent. The relatively high grade of gold in the Mount Charlotte orebody can be explained by the unusually steep temperature-gradient along the fluid-flow path through the vein network.

Keywords: gold deposit, Mount Charlotte, hydrothermal alteration, gold mineralization, fluid inclusions, Kalgoorlie, Australia.

SOMMAIRE

Le gisement aurifère de Mount Charlotte, à Kalgoorlie, en Australie, est fait d'une série de zones minéralisées à fort pendage, dans lesquelles des veines de quartz conjuguées sont entourées d'une auréole à sulfures qui contient la plupart de l'or. Nous distinguons trois types d'altération, dont la distribution est systématique à l'échelle du gisement, avec une auréole riche en pyrite vers le haut et près de la périphérie du gisement, et une auréole à pyrrhotite en profondeur et au centre des zones de montée de la phase fluide. Nous avons analysé les inclusions fluides piégées dans le quartz du stade principal de minéralisation des veines de

[§] E-mail address: terry.mernagh@ga.gov.au

chacun des trois types d'altération afin d'évaluer la présence possible de gradients thermiques et chimiques à l'échelle du gisement. Les assemblages d'inclusions fluides associés à l'altération à faible profondeur et dans les parties plus distales, à pyrite + muscovite, contiennent des inclusions à trois phases H_2O-CO_2 et coexistent avec des inclusions riches en liquide aqueux avec moins de 15% de phase vapeur, en volume. La température d'homogénéisation la plus faible indiquée par les assemblages d'inclusions fluides de cet assemblage est entre 210 et 245°C. Les assemblages d'inclusions fluides des veines de quartz des zones à pyrite + pyrrhotite contiennent des inclusions à deux phases dans le système $H_2O-CO_2-CH_4$ et des inclusions aqueuses riches en liquide. La température d'homogénéisation varie de 240 à 275°C. Les veines entourées d'une gaine à pyrrhotite + albite contiennent des inclusions $H_2O-CO_2-CH_4$ à deux phases et des inclusions aqueuses riches en liquide, dont la température d'homogénéisation la plus faible est dans l'intervalle 260 à 310°C. Nous avons aussi observé une population tardive d'inclusions H_2O-CH_4 secondaires riches en liquide, en association avec l'altération à pyrite + muscovite et pyrrhotite + albite. Ces inclusions s'homogénéisent entre 239 et 286°C. Quoique les intervalles de température se chevauchent, les données sur les inclusions fluides et sur les modes d'altération concordent pour indiquer un gradient important en température entre la base et le sommet du gisement (jusqu'à 100°C / km) pendant la formation du stockwerk de veines et de l'altération au Mount Charlotte. En revanche, la composition chimique de la phase fluide en termes de $H_2O : CO_2 : CH_4 : NaCl$, telle que déterminée par microthermométrie et par microspectrométrie de Raman, ne semble pas varier de façon systématique à l'échelle du gisement, quoique le rapport $CH_4 : CO_2$ a varié largement. D'après ces observations, la déposition de l'or à Mount Charlotte aurait eu lieu par perte de soufre aux dépens des complexes bisulfurés suite aux réactions avec les roches riches en fer des parois, pour produire la pyrrhotite et la pyrite, comme on l'a déjà montré. Ces réactions dépendent fortement de la température. La teneur relativement élevée en or du gisement de Mount Charlotte dépendrait d'un gradient thermique inhabituellement abrupt au cours de la montée de la phase fluide le long du réseau de veines.

(Traduit par la Rédaction)

Mots-clés: gisement aurifère, Mount Charlotte, altération hydrothermale, minéralisation en or, inclusions fluides, Kalgoorlie, Australie.

INTRODUCTION

Relatively CO_2 -rich, ore-forming fluids have long been recognized as characteristic of lode-gold deposits in sub-amphibolite-facies rocks (Kerrick & Fyfe 1981, Neall & Phillips 1987, Robert & Kelly 1987, Ho *et al.* 1990a, b, Yeats & Vanderhor 1998, Ridley & Diamond 2000). Estimates of CO_2 in the initial ore-forming fluid from both thermodynamic models and fluid-inclusion measurements (Ho *et al.* 1990b) indicate $X(CO_2)$ values ranging from 0.05 to 0.3. Gradients in $X(CO_2)$ exert a major control on the stability of carbonate and silicate minerals in alteration haloes around greenschist-facies lode-gold deposits (Diamond & Marshall 1990, Mikucki & Ridley 1993).

The subsequent study of gold deposits in terranes at higher metamorphic grade has led to the proposal of the "crustal continuum model" (Groves *et al.* 1992), in which mineralization resulted from ore-fluids issuing from a deep source rising up through vertically extensive hydrothermal systems through the crust. The occurrence of Archean lode-gold deposits over a large vertical range in the crust has important implications for fluid sources and genetic models for these deposits. Within a "crustal continuum" model of fluid flow, changes in the composition of the ore fluids would be expected as they rise through the crust. Crustal-scale fluid flow, decompression and cooling lead to chemical disequilibrium between progressively focussed fluids, as evidenced by metamorphic-grade-dependent types of alteration on the district scale (Witt 1991), but measurable temperature-gradients at the mine to vein scale are rarely recorded in Archean lode-gold deposits (Phillips

& Groves 1983, Robert & Kelly, 1987, Channer & Spooner, 1991, Ridley *et al.* 1994).

The Mount Charlotte gold deposit in the Eastern Goldfields Province of Western Australia is one of the oldest bulk-mining operations in the Kalgoorlie gold field (Clout *et al.* 1990). Mineralization associated with sulfide-rich alteration of a gabbro sill along a continuous network of veins extends at least 1 km beneath the surface. Ore grades in the upper part of the deposit (*e.g.*, the Mount Charlotte orebody) were 4.9 g/t, which is relatively high for a bulk-mineable deposit in which most of the gold occurs in disseminated form (Clout *et al.* 1990). This has made Mount Charlotte a very profitable mine for a number of decades. Several investigators (Clark 1980, Clout *et al.* 1990) have identified three distinct alteration-induced haloes surrounding the veins at Mount Charlotte, and Mikucki & Heinrich (1993) have shown that the mineralogy of these haloes records a vertical as well as lateral zonation within the deposit.

Building on previous reports of relatively well-preserved fluid inclusions at Mount Charlotte (Clark 1980, Ho 1986, Ho *et al.* 1990a), we investigate the spatial variation of fluid-inclusion properties, in an attempt to explain the mineralogical variation of alteration on the deposit scale and its relation to the mechanisms of precipitation of gold in an otherwise typical Archean mesothermal lode-gold deposit.

GEOLOGICAL SETTING

The Mount Charlotte deposit is situated within the western limb of the Kalgoorlie syncline (Fig. 1), which forms part of the Archean Norseman-Wiluna green-

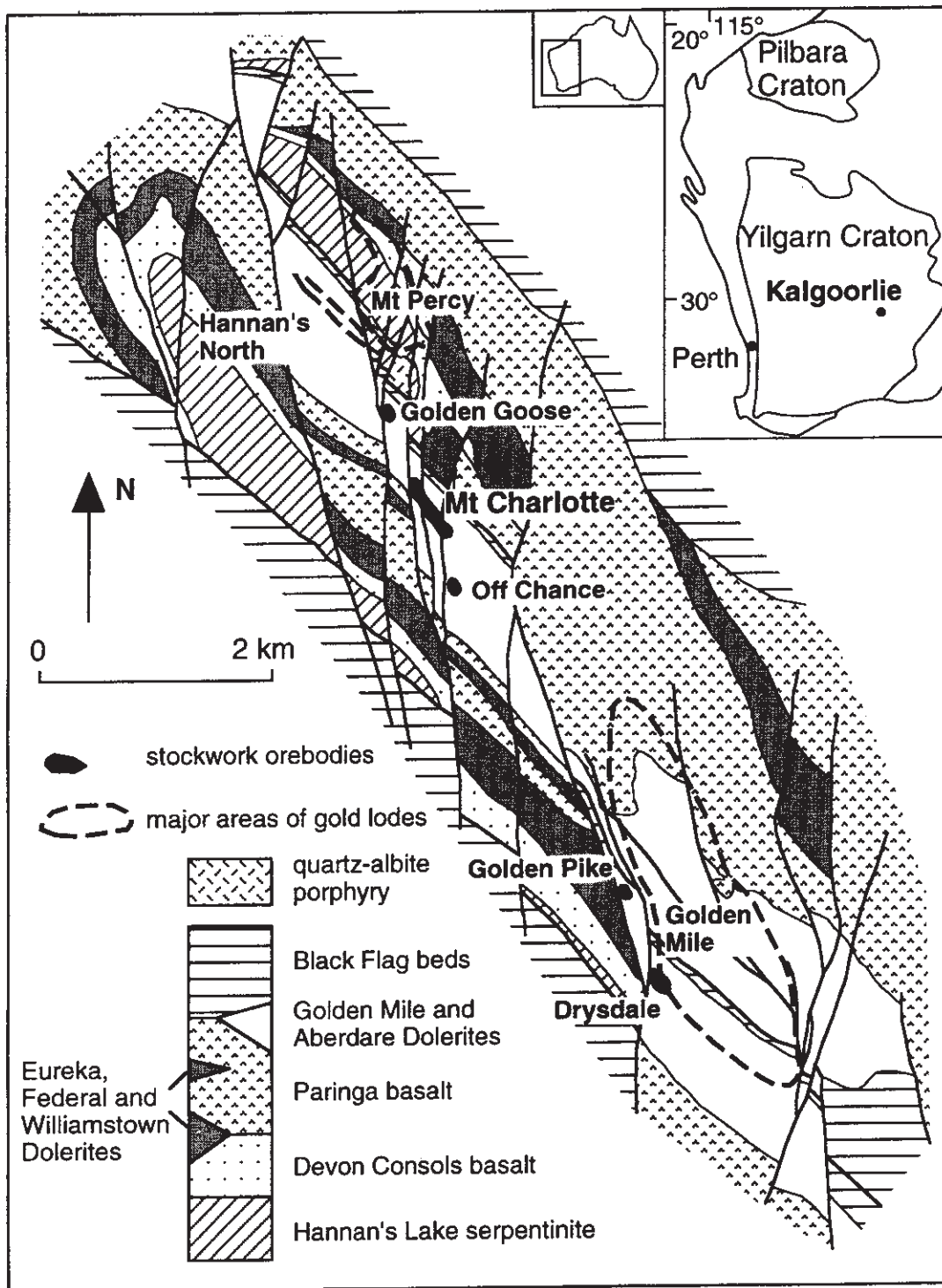


FIG. 1. Geology of the Kalgoorlie gold field. Illustration from Ridley & Mengler (2000, Fig. 1), reprinted with permission of *Economic Geology*.

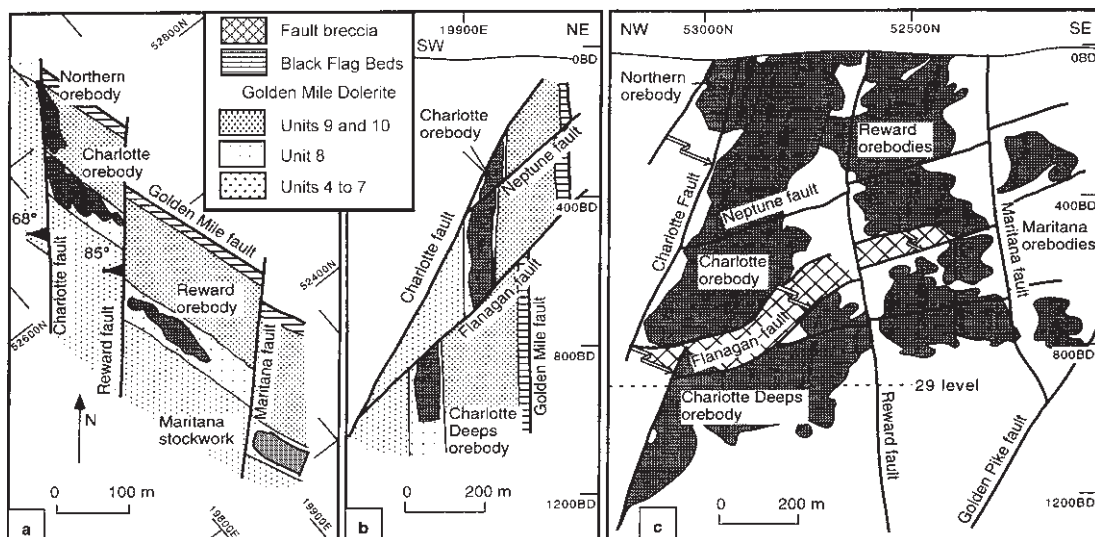


FIG. 3. The Mount Charlotte deposit in (a) plan view at the 3 level, (b) cross section at 52850 m N, and (c) schematic northwest-southeast long section projected onto 19900 m E. Regions shaded dark grey depict the area of the gold orebodies. The Charlotte fault appears three times on the long section to show its positions adjacent to the Northern Charlotte, and Charlotte Deeps orebodies. Cross hatching shows the projection of the Flanagan Fault between the base of the Charlotte orebody and the top of the Charlotte Deeps orebody. Illustration from Ridley & Mengler (2000, Fig. 2), reprinted with permission of *Economic Geology*.

partly filled by calcite. Although this stage does not represent a distinct "stage" of vein development, it is mineralogically distinct from Stage 2. Numerous inclusions of carbonate, chlorite and pyrite occur in the outer growth zones of the crystals.

The structural controls on the formation of these vein-stockwork deposits, and in particular, the roles of the bounding faults, are subjects of ongoing debate. The most intense mineralization in the Charlotte orebody is adjacent to the Charlotte fault. Travis *et al.* (1971) suggested that the veins occupy tension fractures related to fault movement. Clark (1980) and Clout *et al.* (1990) also argued that the stockwork veins formed synchronously with the late stages of movement on the faults. Scott (1997) suggested that the formation of two sets of quartz veins was due to high fluid pressures and periodic reorientation of stress after fault slip. Ridley & Mengler (2000) argued that the major sets of faults are unfavorably oriented for slip or dilation, and suggested that the lack of fault activity during ore-fluid flow promoted the formation of a network of open veins at Mount Charlotte. They suggested that permeability resulted from fracturing under high fluid pressures before shear-induced or hybrid extensional-shear reactivation of faults. In their model, the paths of fluid flow and the location of the orebodies are controlled by the rheology of Unit 8, and by the three-dimensional geometry of impermeable faults and fault-bounded blocks of rock.

ALTERATION

Throughout the deposit, ~90% of the gold is located on the vein walls and in the haloes of pyritic veins, typically occurring as 5 to 15 μm grains either filling fractures in pyrite or as blebs on the contact between pyrite grains and gangue minerals. Clark (1980) identified three distinct types of alteration haloes surrounding the Mount Charlotte veins, on the basis of differences in the sequence of mineralogical changes that occur in each halo. Systematic variations in the distribution of these three types of contrasting alteration were also reported. The overall mineralogical changes for each alteration assemblage are summarized in Figure 4.

Pyrite-muscovite alteration haloes show a particularly sharply bounded inner zone representing the complete conversion of host-rock epidote – chlorite – magnetite – calcite – ilmenite to a bleached proximal zone composed of ankerite – white mica – rutile – pyrite assemblage with rich gold mineralization. An intervening zone of distal alteration includes chlorite with ilmenite, ankerite and minor pyrite, occurring within 50–100 cm of vein margins.

In pyrite-pyrrhotite alteration haloes, the inner bleaching zone is similar, but pyrrhotite appears in the outer diffuse halo in chlorite+ankerite-bearing rocks up to 1 m from the pyrite – white mica bleaching front. Pyrrhotite – albite alteration haloes locally contain py-

rite as the most vein-proximal sulfide, in some cases as euhedral crystals growing with Stage-1 vein quartz from the wallrock toward the vein opening, but the haloes are characterized by pyrrhotite as the dominant Fe-sulfide in the bleached halo, as well as in the more distal chlorite-bearing zone. In contrast to pyrite-muscovite and pyrite-pyrrhotite alteration, white mica in the pyrrhotite-albite haloes occurs mainly in the more distal chlorite-dominant alteration zones, whereas albite is added and most prominent in the proximal bleached zone. Ilmenite can also be found as relict, partially replaced grains within the proximal bleached zones of pyrite-pyrrhotite and pyrrhotite-albite alteration haloes.

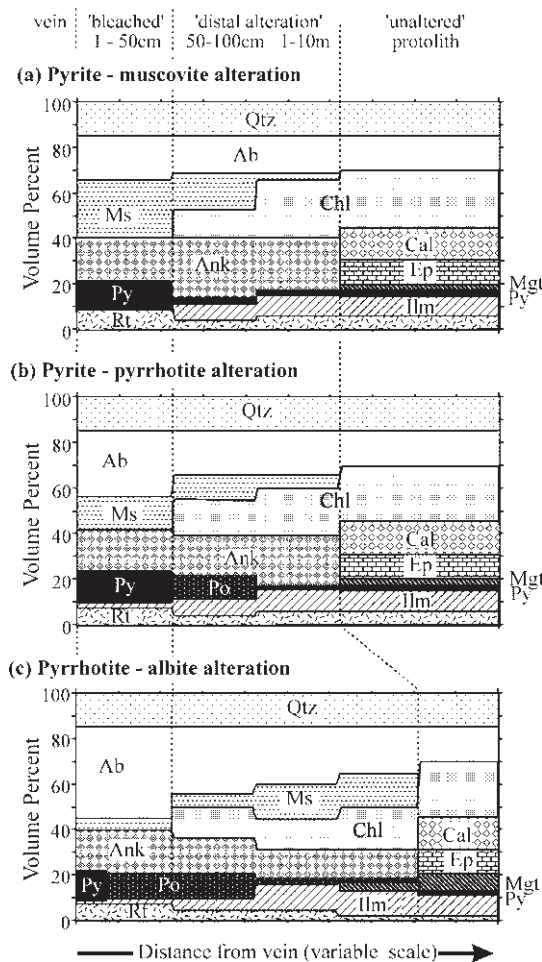


FIG. 4. A graphical representation of the estimated average mineralogy of the three types of alteration observed at Mount Charlotte. Symbols: Qtz: quartz, Ab: albite, Ms: muscovite, Chl: chlorite, Cal: calcite, Ank: ankerite, Ep: epidote, Py: pyrite, Po: pyrrhotite, Ilm: ilmenite, Rt: rutile, and Mgt: magnetite.

The three-dimensional distribution of these distinct alteration haloes has been recorded within the Charlotte and Charlotte Deeps orebodies, by underground mapping of selected horizontal sections, and using drillcore in a composite vertical section (Mikucki & Heinrich 1993; Figs. 5, 6). Distinct regions of contrasting types of alteration haloes define a pattern of concentric shells. As illustrated in Figure 5, pyrrhotite-albite alteration haloes dominate within the core of the stockwork and at the deeper levels of the mine. Pyrite-pyrrhotite alteration haloes occur in the distal, isolated veins in the Charlotte Deeps, but are most common along the periphery of the orebodies at intermediate levels and dominate the economic ore-zone at the highest levels of the deposit. Pyrite-muscovite haloes, although locally highly gold-mineralized, mostly occur at the periphery and outside of the bulk-mineable orebody.

Mine-scale alteration boundaries locally transgress lithological contacts, and thus rule out compositional variations in the protolith as the main control on zoning of alteration assemblages within the orebodies. The alteration zones are centered on areas of highest density of veins within the stockwork rather than emanating from the Charlotte Fault, and thus preclude the latter as a major fluid-flow pathway (at least above the Flanagan Fault). In contrast, veining along parts of the Flanagan Fault exhibit the same patterns of alteration zoning as noted above, with pyrrhotite-albite alteration extending to unusually high levels. Mikucki & Heinrich (1993) have therefore suggested that parts of the Flanagan Fault may have acted as a fluid channelway linking the Charlotte Deeps with the Charlotte orebody.

PETROGRAPHY OF FLUID INCLUSIONS

To determine whether the three different styles of alteration mentioned above are associated with fluids of different temperature, pressure or chemical composition, samples were selected according to the type of alteration halo surrounding the quartz veins across the entire depth of the deposit. A total of 72 samples were examined petrographically, but only 3-6 samples from each type of alteration across a maximum possible depth-range were selected for detailed analysis of the fluid inclusions.

In this study, we have concentrated on veins that are less than 5 cm wide with distinctive alteration-induced haloes, in order to avoid some of the complexities of the larger veins. The outer selvages of Stage-1 quartz (Clark 1980) are very narrow (typically < 1 mm) in these samples, and no fluid inclusions of a suitable size for microthermometry were found within this zone. Therefore, all inclusions examined in this study were taken from the relatively clear and weakly strained quartz crystals in Stage-2 quartz. This quartz probably represents the most voluminous phase of fluid flow, and inclusions in this stage best define the larger-scale conditions for inflow of mineralizing fluids at Mount

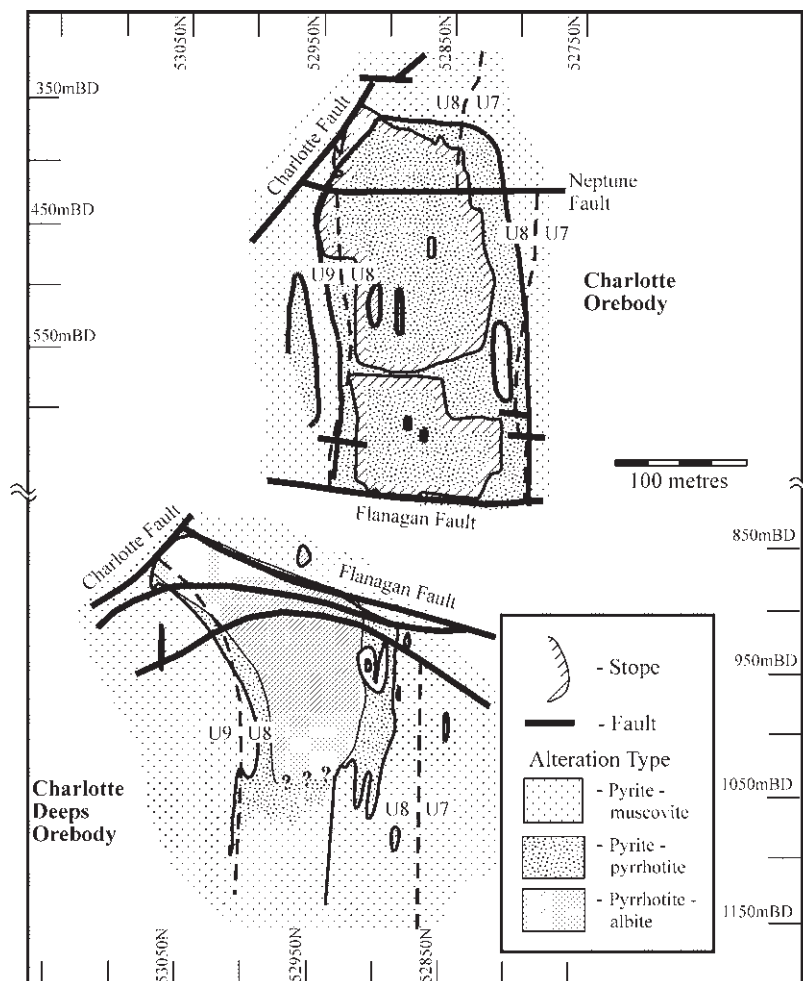


FIG. 5. Distribution of alteration haloes in a composite vertical section through the Charlotte orebody (Q Drill Section) above, and the Charlotte Deeps orebody (136 Drill Section) below, the Flanagan Fault. Both sections cut approximately through the center of the vein stockwork, but are offset out of the plane of the figure owing to the displacement of the Unit 8 granophyre along the early Flanagan Fault (modified from Mikucki & Heinrich 1993).

Charlotte. Stage-3 quartz is not present in the narrow quartz veins selected for this study.

Stage-2 quartz contains an abundance of fluid inclusions in densely packed arrays, and hence, it was impossible to distinguish between primary and secondary inclusions using the criteria outlined in Roedder (1984). For this reason, our studies focused on "Fluid Inclusion Assemblages (FIA)" as defined by Goldstein & Reynolds (1994). An FIA corresponds to a limited number (typically between 10 and 20) of inclusions of similar petrographic character formed at the same time,

which may serve as the test population to evaluate the homogeneity of microthermometric data (notably T_h). FIA correspond closely to "Groups of Synchronous Inclusions (GSI)" as defined by Touret (2001).

The FIA used in this study consisted of three-dimensional clusters of inclusions that are assumed to have formed contemporaneously owing to their close spatial association. In order to obtain the maximum temperature of the fluids in Stage-2 quartz, the phase ratios observed within the inclusions at 25°C were used to predict which FIA were trapped at the highest temperatures.

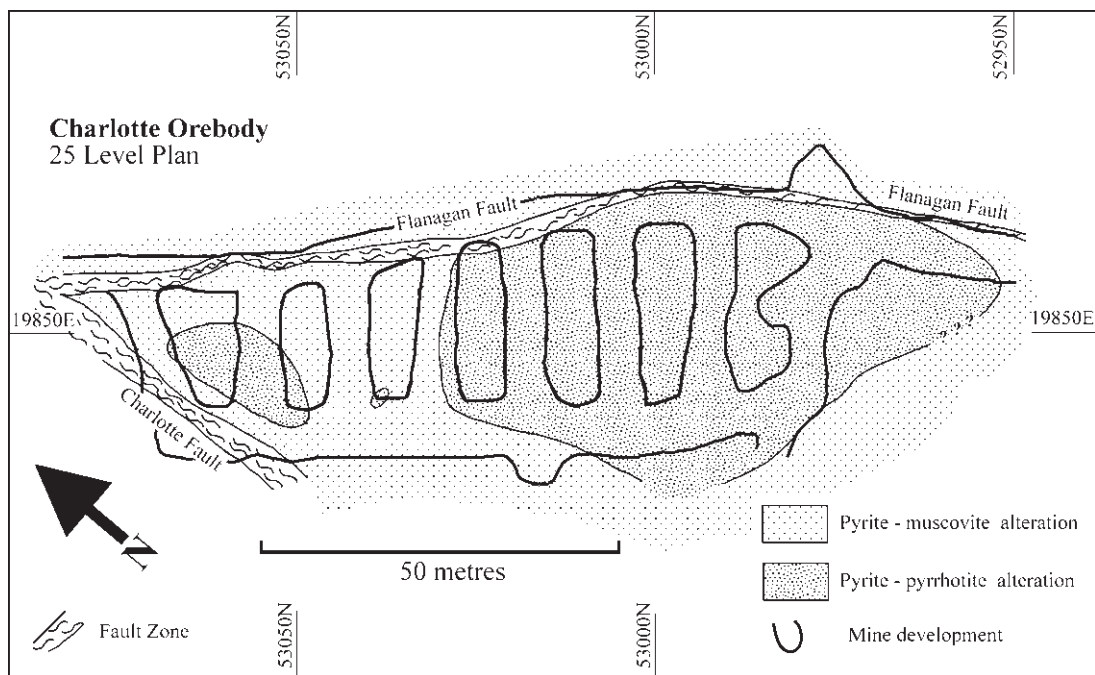


FIG. 6. Distribution of alteration zoning in a horizontal section through the Charlotte orebody at the 25 level (765 mBD) (modified from Mikucki & Heinrich 1993).

These groups contain liquid-rich fluid inclusions with the highest vapor content and vapor-rich inclusions with the highest percentage of liquid. The Leica Q500MC image-analysis software was used to accurately determine areal proportions of the respective phases in the fluid inclusions and to convert them into volume equivalents assuming an approximately ellipsoidal shape of the inclusions.

Four types of fluid inclusions have been recognized in the veins at Mount Charlotte by a combination of petrographic observation and Raman microprobe analysis (below): 1) three-phase $\text{H}_2\text{O}-\text{CO}_2$ inclusions, containing 10–70% of liquid water and a two-phase bubble of liquid + vapor CO_2 . Minor amounts of CH_4 may be present in the carbonic phases, 2) liquid-rich, aqueous inclusions with less than 15 vol.% vapor, 3) two-phase $\text{H}_2\text{O}-\text{CO}_2-\text{CH}_4$ inclusions, with various ratios of CO_2 and CH_4 and a carbonic phase comprising 30–100 vol.%, and 4) liquid-rich $\text{H}_2\text{O}-\text{CH}_4$ inclusions containing approximately 5 vol.% methane-rich vapor.

The veins with pyrite–muscovite alteration haloes contain both three-phase $\text{H}_2\text{O}-\text{CO}_2$ inclusions and liquid-rich, aqueous inclusions (Fig. 7a). These inclusions are generally less than 15 μm in diameter. The larger inclusions typically have an irregular shape, whereas the smaller, liquid-rich inclusions are more rounded. Quartz veins associated with pyrite–pyrrhotite alteration con-

tain FIAs with liquid-rich, aqueous inclusions and two-phase $\text{H}_2\text{O}-\text{CO}_2-\text{CH}_4$ inclusions (Fig. 7b) up to 30 μm in size. Veins with pyrrhotite–albite alteration also contain liquid-rich, aqueous inclusions and two-phase $\text{H}_2\text{O}-\text{CO}_2-\text{CH}_4$ inclusions (Fig. 7c). The two-phase $\text{H}_2\text{O}-\text{CO}_2-\text{CH}_4$ inclusions in these veins typically have a higher vol.% of carbonic phase than those in pyrite–pyrrhotite alteration. Many of the larger inclusions in veins with pyrrhotite–albite alteration have an irregular shape and features indicative of partial decrepitation (*cf.* Pecher 1981, Bodnar *et al.* 1989, Ayllón *et al.* 2003). Inclusions showing signs of partial decrepitation were avoided where possible, but the data still show some evidence for post-entrapment changes (see below).

Liquid-rich $\text{H}_2\text{O}-\text{CH}_4$ inclusions are quite rare (Fig. 7d). These inclusions are typically small (<10 μm), with roundish to negative crystal shapes, and they occur in veins with either pyrite–muscovite and pyrrhotite–albite alteration haloes as trails that cut across quartz-grain boundaries. Therefore, they are interpreted as late, post-mineralization, secondary inclusions.

ANALYTICAL TECHNIQUES

Microthermometric data were obtained using either a modified USGS gas-flow heating–freezing stage or a Linkam THM 600 heating–freezing stage. Both stages

were calibrated with the same series of synthetic fluid inclusions of known composition. A heating rate of 1°C per minute was used to record phase changes below 30°C, whereas a heating rate of 5°C per minute was used for phase changes above this temperature. Hence, low-temperature phase changes are accurate to $\pm 0.2^\circ\text{C}$, whereas temperatures above 30°C have an estimated accuracy of $\pm 2^\circ\text{C}$. Salinity, mole fractions and bulk density of each inclusion were calculated using the program MacFlinCor (Brown & Hagemann 1995). The equations from Bodnar & Vityk (1994) were used for aqueous inclusions, whereas the equation of state from Jacobs &

Kerrick (1981) was used for CO_2 -bearing inclusions. Salinities for CO_2 - and CH_4 -bearing inclusions were calculated from the melting temperature of the clathrate using the equations of Bakker (1997).

Laser Raman microprobe analyses were obtained with a Microdil 28 spectrometer (Liu & Mernagh 1990) using 40 mW (at the sample) of 514.5 nm laser excitation from a Spectra Physics 2020 5W argon laser. Spectra were typically obtained after 10 accumulations with a 5-second integration time and an approximately 5 cm^{-1} spectral bandpass. The Raman spectra were calibrated using Ar^+ plasma and neon emission lines. The ratio of

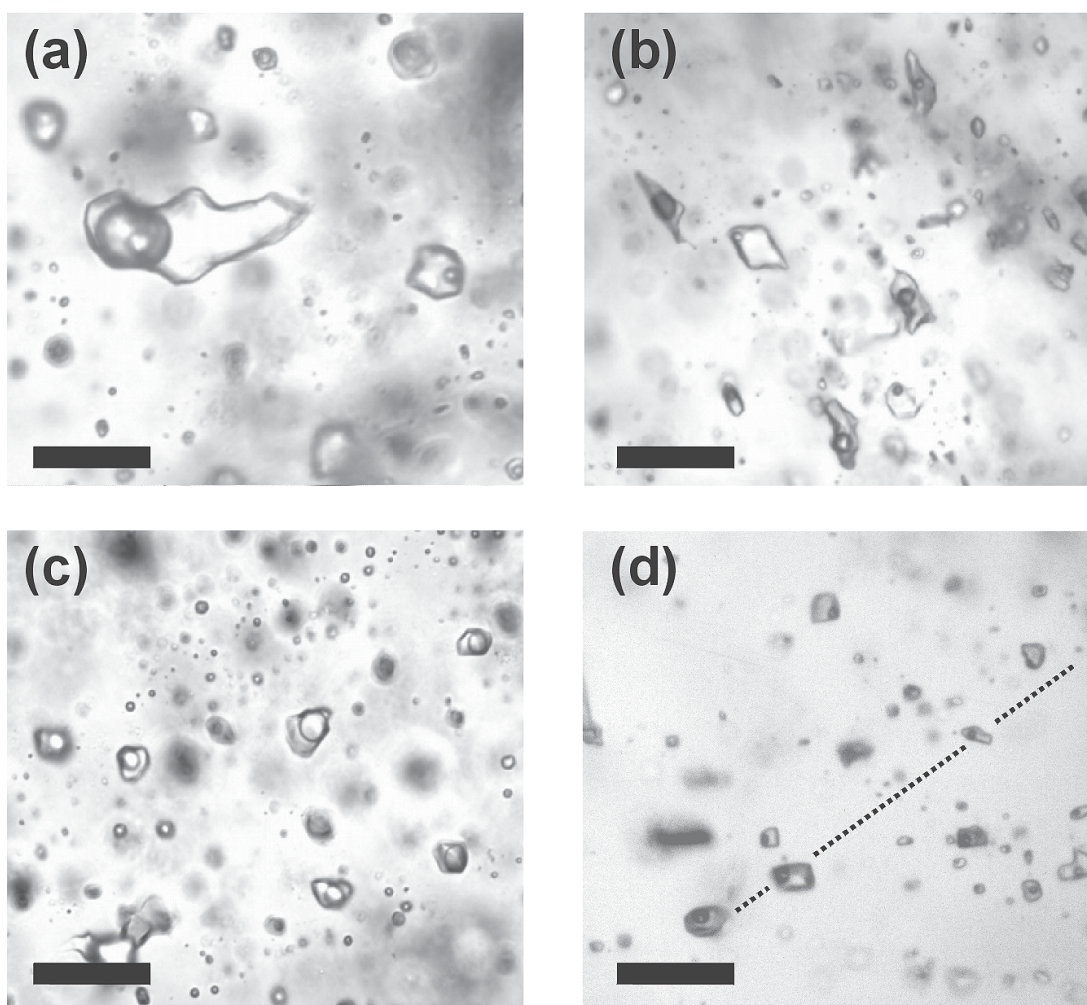


FIG. 7. Photomicrographs of fluid inclusions at Mount Charlotte. (a) Coexisting three-phase $\text{H}_2\text{O}-\text{CO}_2$ inclusions and liquid-rich aqueous inclusions in quartz associated with pyrite–muscovite alteration; scale bar: 10 μm . (b) Coexisting two-phase $\text{H}_2\text{O}-\text{CO}_2-\text{CH}_4$ inclusions and liquid-rich aqueous inclusions in quartz associated with pyrite–pyrrhotite alteration. Scale bar: 20 μm . (c) Two-phase $\text{H}_2\text{O}-\text{CO}_2-\text{CH}_4$ inclusions in quartz associated with pyrrhotite–albite alteration. Scale bar: 20 μm . (d) Liquid-rich $\text{H}_2\text{O}-\text{CH}_4$ inclusions in quartz associated with pyrrhotite–albite alteration. Scale bar: 10 μm .

gaseous species in the vapor phase was calculated using the method described by Dubessy *et al.* (1989), and the following "quantification factors" were calculated as outlined in Pasteris *et al.* (1988): CO₂ = 1.3 and CH₄ = 7.6. Raman detection limits are dependent on instrumental sensitivity and the partial pressure of each gas, but are estimated to be about 0.15 MPa for CO₂ and 0.03 MPa for CH₄ under the conditions of this study.

RESULTS

Previous fluid-inclusion data from Clark (1980), Ho (1986) and Ho *et al.* (1990a) are summarized in Table 1. These investigators have measured fluid inclusions in all three stages of vein quartz defined by Clark (1980), but they have not attempted to relate the data to the styles of alteration surrounding these veins. Mostly three-phase H₂O–CO₂ inclusions were observed, with two-phase H₂O- and CH₄-bearing inclusions only being reported in Stage-3 quartz. Measurements of salinity for fluids in Stage-3 quartz vary from 2.0 to 4.2 wt.% NaCl eq. in carbonic inclusions, and from 4.1 to 5.5 wt.% NaCl eq. in aqueous inclusions. Temperatures of total homogenization range from 210 to 360°C, and pressures of trapping (based on the system H₂O–CO₂) vary from 1.5 to 2.2 kbar (Ho *et al.* 1990a).

Fluid inclusions in veins with a pyrite–muscovite alteration halo

The microthermometric data from Stage-2 quartz veins in this study are summarized in Table 2 and Figures 8–11. FIAs associated with pyrite–muscovite alteration have a salinity of less than 7 wt.% NaCl eq. (Fig. 8a) with a mode at 3 wt.% NaCl eq. The temperature of final melting of three-phase H₂O–CO₂-bearing inclusions (Fig. 9a) is close to –56.6°C, which indicates that these inclusions contain little or no CH₄, as con-

firmed by laser-Raman microprobe analysis (see below). Homogenization temperatures ($T_{h\ L+V\rightarrow L}$) for liquid-rich, aqueous inclusions range from 98 to 312°C, and generally overlap with those for the three-phase H₂O–CO₂ inclusions, which range from 210 to 316°C (Fig. 10), with the exception of a small group of liquid-rich, aqueous inclusions that homogenize below 200°C. This latter group may represent a separate population of inclusions related to a lower-temperature episode of fluid flow through these veins.

The coexistence of both liquid- and vapor-rich inclusions and the overlapping temperatures of inclusions indicate that fluid immiscibility (phase separation) occurred in these veins. The majority of three-phase H₂O–CO₂ inclusions contain between 5 and 15 mol.% CO₂, which would equate to pressures of trapping between 0.8 and 3 kbar according to the data of Gehrig *et al.* (1986) for a system with 6 wt.% NaCl.

The results of the laser-Raman microprobe analyses are summarized in Table 2 and Figure 12. In most cases, only CO₂ was detected in the carbonic phase of the three-phase H₂O–CO₂ inclusions with pyrite–muscovite alteration. However, a few of the more vapor-rich inclusions were found to contain minor amounts of CH₄ (2 mole % or less), but no N₂ was detected. This finding is in good agreement with the temperature of final melting of CO₂ for these inclusions (see above), which is close to the values expected for pure CO₂.

Fluid inclusions in veins with a pyrite–pyrrhotite alteration halo

FIAs in veins with pyrite–pyrrhotite alteration have a more variable liquid:vapor ratio, but maximum vapor contents are only around 60 vol.%, and the average bulk density calculated from the MacFlinCor program is 0.91 g/cm³. Such inclusions have a salinity of less than 8 wt.% NaCl eq. (Fig. 8b), with the liquid-rich inclusions

TABLE 1. A SUMMARY OF PREVIOUS FLUID-INCLUSION DATA FROM MOUNT CHARLOTTE*

Vein style	Phases	Fluid composition	Density (g/cm ³)	T _h (Total) (°C)	Pressure of trapping (kbar)
Stage-1 quartz	Three-phase H ₂ O–CO ₂ (30–40 vol.% CO ₂)	No data on salinity CH ₄ not detected	0.80–0.85	300–360	1.6–2.1
Stage-2 quartz	Three-phase H ₂ O–CO ₂ (40–60 vol.% CO ₂)	No data on salinity CH ₄ not detected	0.75–0.85	210–325	1.6–2.2
Stage-3 quartz	Three-phase H ₂ O–CO ₂ (40–60 vol.% CO ₂)	2.0–4.2 wt.% NaCl eq. CH ₄ not detected	0.80–0.85	285–320	1.5–2.0
Stage-3 quartz	Two-phase H ₂ O (15–30 vol.% vapor)	4.1–5.5 wt.% NaCl eq.	~0.8	265–290	Not determined
Stage-3 quartz	Two-phase H ₂ O–CO ₂ –CH ₄ (40–75 vol.% carbonic phase)	No data on salinity H ₂ O–CO ₂ –CH ₄ and H ₂ O–CH ₄ with up to 20 wt.% CH ₄	Not determined	Not determined	Not determined

* Taken from Ho *et al.* (1990a).

TABLE 2. MICROTHERMOMETRIC AND LASER-RAMAN MICROPROBE DATA FOR FLUID INCLUSIONS IN THE DIFFERENT STYLES OF ALTERATION AT MOUNT CHARLOTTE

Alteration or Inclusion type	Vapor/carbonic phase (vol.%)	T _m (Car) ^a (°C)	T _m (Ice) (°C)	T _m (Clathrate) (°C)	T _h (Car) ^a (°C)	T _h (Total) (°C)	X(CO ₂) Vap ^b	X(CH ₄) Vap ^b
Pyrite – muscovite								
Three-phase H ₂ O–CO ₂	30–90 (n = 29)	–57.4 to –56.6 (–56.7)		8.0 to 8.7 (8.3) ^c	16.0 to 20.5 (17.8)	210–302.8 (191) L ^d	0.98–1.0 (0.998)	0.0–0.02 (0.002)
Three-phase H ₂ O–CO ₂	30–90 (n = 19)	–57.5 to –56.6 (–56.8)		7.9 to 8.7 (8.1)	25.7 to 30.9 (29.2)	212.0–315.6 (252) V	0.98–1.0 (0.994)	0.0–0.02 (0.006)
Liquid-rich, aqueous	5–10 (n = 32)		–1.6 to –3.1 (–2.7)			98.0–312.5 (194.4) L		
Pyrite – pyrrhotite								
Liquid-rich, aqueous	10–25 (n = 24)		–1.0 to –4.2 (–2.8)			220.4–282.9 (217) L		
Two-phase H ₂ O–CO ₂ –CH ₄	30–60 (n = 26)	–66.4 to –56.6 (–60.7)		9.0 to 11.0 (9.5)	10.5 to 14.3 (12.8)	218.1–314.6 (273) L	0.05–1.0 (0.712)	0.0–0.85 (0.288)
Two-phase H ₂ O–CO ₂ –CH ₄	30–60 (n = 21)	–64.4 to –58.8 (–61.5)		9.5 to 11.9 (9.9)	11.6 to 16.7 (14.1)	251.8–322.7 (287) V	0.0–1.0 (0.660)	0.0–1.0 (0.340)
Pyrrhotite – albite								
Liquid-rich, H ₂ O	5–10 (n = 59)		–2.0 to –6.2 (–3.5)			202.2–440.1 (295) L		
Two-phase H ₂ O–CO ₂ –CH ₄	30–100 (n = 38)	–62.8 to –57.1 (–59.3)		7.6 to 10.0 (8.8)	–10.0 to 26.0 (12.7)	235.3–438.9 (298) L	0.74–0.96 (0.871)	0.04–0.26 (0.129)
Two-phase H ₂ O–CO ₂ –CH ₄	30–100 (n = 27)	–63.2 to –57.1 (–59.2)		7.9 to 12.3 (10.2)	8.8 to 15.3 (13.1)	238.3–437.9 (315) V	0.9–0.96 (0.931)	0.04–0.09 (0.069)
Liquid-rich, H ₂ O–CH ₄	5–10 (n = 12)			14.8 to 16.7 (15.0)	–87.8 to –86.1 (–87.0)	239.0–286.3 (254) L	0.0–0.34 (0.072)	0.66–1.0 (0.928)

^a The carbonic phase may consist of both CO₂ and CH₄. The carbonic phase of all inclusions homogenized to liquid.

^b Mole fraction of CO₂ or CH₄ in the vapor phase as determined by laser-Raman microprobe analysis.

^c The quoted figures represent the range of the data, and the average value is given in parentheses.

^d L and V denote homogenization to the liquid and vapor phase, respectively.

again exhibiting a higher salinity than vapor-rich inclusions (Fig. 10). Two-phase H₂O–CO₂–CH₄ inclusions exhibit a temperature of final melting of CO₂ ranging from –66.4° to –56.6° C (Fig. 9b), which indicates that variable amounts of CH₄ (as confirmed by laser-Raman analysis) are present in the carbonic phase of these inclusions. Most of the vapor-rich H₂O–CO₂–CH₄ inclusions decrepitated before total homogenization, but as shown in Figures 10 and 11, there is overlap and good agreement for the homogenization temperatures of both the liquid- and vapor-rich inclusions.

Raman-microprobe analysis of FIAs from veins with pyrite–pyrrhotite alteration showed that the vapor phase contains variable amounts of CO₂ and CH₄. The majority of inclusions have vapor-phase contents of CH₄ ranging from 11 to 61 mole % (Fig. 12). However, a small

number of other inclusions containing either <5 mole % or >75 mole % CH₄ also were observed, but these may represent the rare occurrence of two-phase H₂O–CO₂ or secondary, liquid-rich, H₂O–CH₄ inclusions in veins with pyrite–pyrrhotite alteration. The large variation in CO₂:CH₄ ratio indicates fluctuating *f*(O₂) conditions, as shown by the precipitation of pyrite within the bleached zone and of pyrrhotite in the more distal alteration (Fig. 4).

Fluid inclusions in veins with a pyrrhotite–albite alteration halo

Fluid inclusions in veins with pyrrhotite–albite alteration have a salinity ranging from 1 to 9 wt.% NaCl eq., with a clear mode at 5 wt.% NaCl eq. (Fig. 8c).

These inclusions show a depression in the temperature of final melting of CO_2 to values as low as -63.2°C , indicating that they contain variable amounts of CH_4 . Many of the inclusions decrepitate before total homogenization, but the remaining liquid-rich, aqueous inclusions and two-phase $\text{H}_2\text{O}-\text{CO}_2-\text{CH}_4$ inclusions show general overlap of their homogenization temperatures (Figs. 10, 11). The plot of homogenization temperature versus salinity (Fig. 10) also shows that liquid-rich, aqueous inclusions generally have higher salinities than the two-phase $\text{H}_2\text{O}-\text{CO}_2-\text{CH}_4$ inclusions. This is a consequence of phase separation, as unmixing of a homogeneous $\text{H}_2\text{O}-\text{CO}_2-\text{CH}_4-\text{NaCl}$ fluid will result in the formation of a lower-salinity CO_2-CH_4 -rich phase and

a higher-salinity aqueous phase (Ramboz *et al.* 1982). Raman analysis of two-phase $\text{H}_2\text{O}-\text{CO}_2-\text{CH}_4$ inclusions in veins with pyrrhotite-albite alteration show that the carbonic phase contains up to 26 mole % CH_4 , which corresponds well with the microthermometric data given in Table 2.

The homogenization temperatures of secondary, liquid-rich $\text{H}_2\text{O}-\text{CH}_4$ inclusions are also shown in Figure 11 for comparison. These inclusions have an average temperature of homogenization that is lower than that of most inclusions in veins with pyrrhotite-albite alteration, and they also have a markedly more methane-rich vapor phase. These secondary inclusions were found to contain greater than 66 mole % CH_4 in the vapor phase, with the majority containing greater than 95 mole % CH_4 (Fig. 12).

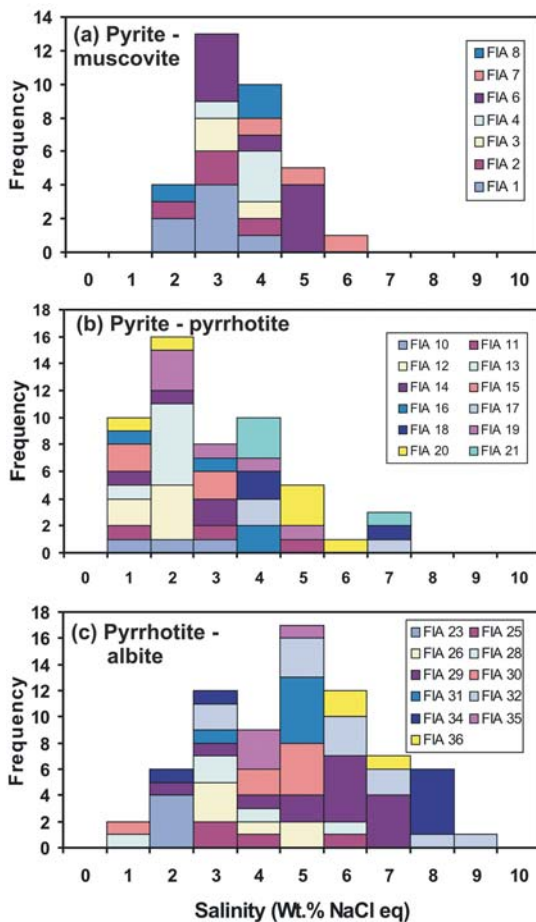


FIG. 8. Histograms showing the salinity of vapor- and liquid-rich fluid inclusions in veins with (a) pyrite-muscovite, (b) pyrite-pyrrhotite, and (c) pyrrhotite-albite alteration haloes. The different colors depict data obtained from different Fluid Inclusion Assemblages (FIAs).

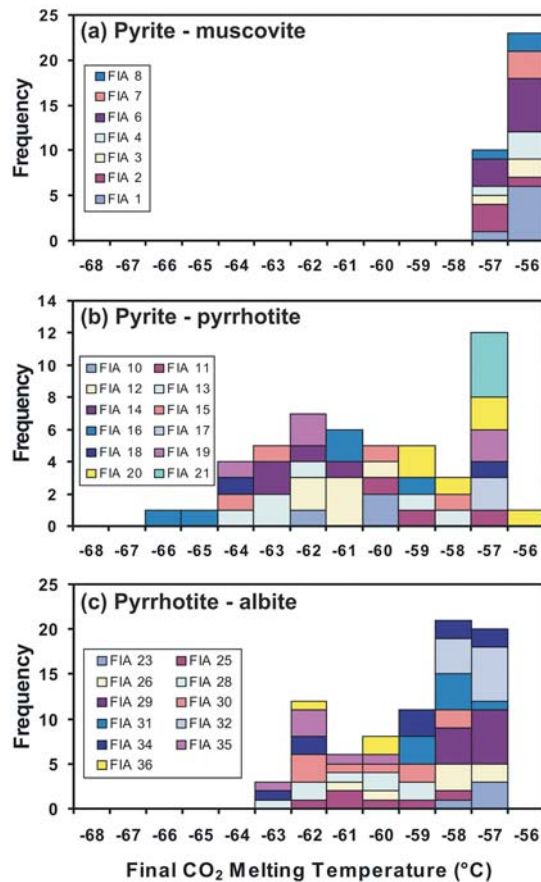


FIG. 9. Histograms showing the temperature of final melting of the carbonic phase for (a) pyrite-muscovite, (b) pyrite-pyrrhotite, and (c) pyrrhotite-albite alteration haloes. The different colors depict data obtained from different Fluid Inclusion Assemblages (FIAs).

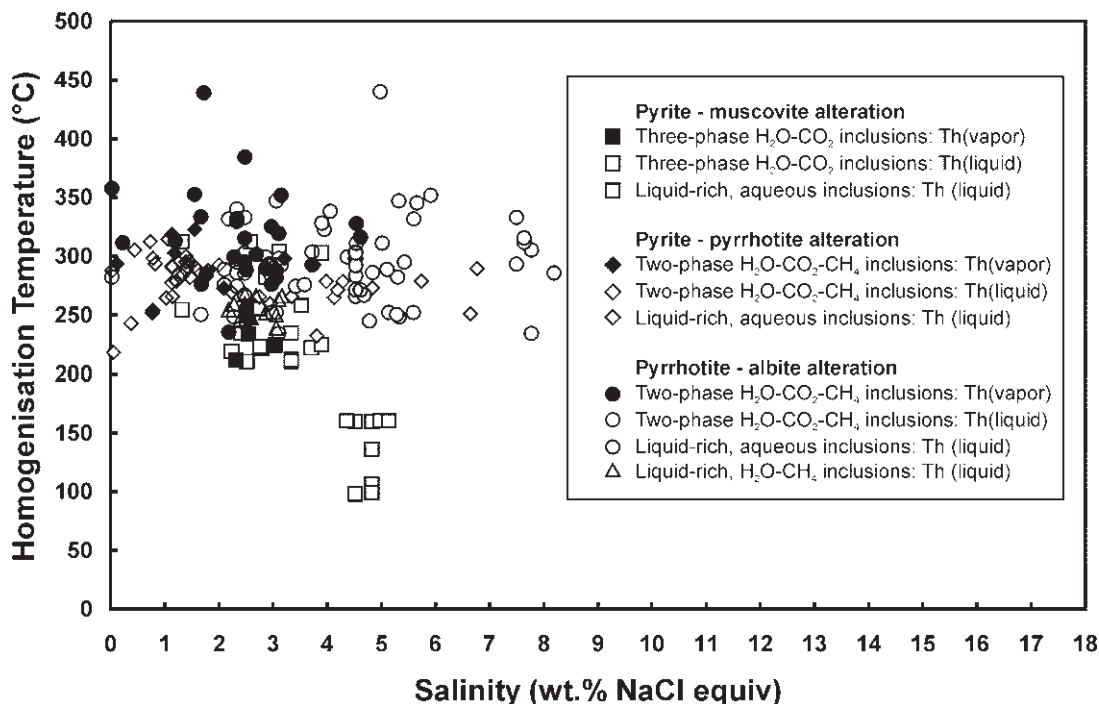


FIG. 10. Plot of temperature of total homogenization *versus* salinity for the various inclusions observed in the three alteration haloes at Mount Charlotte.

The variation in CH₄ content for three-phase H₂O-CO₂ and two-phase H₂O-CO₂-CH₄ inclusions is shown in more detail in Figure 13. The majority of carbonic inclusions in veins with pyrite-muscovite alteration have molar volumes above 60 cm³ and contain little or no CH₄. In contrast, carbonic inclusions in veins with pyrite-pyrrhotite alteration have variable molar volumes and exhibit a large range of CH₄ concentrations. Two-phase H₂O-CO₂-CH₄ inclusions in veins with pyrrhotite-albite alteration also have CH₄ contents ranging from <5 to >30 mole % and show the largest variation in molar volume. Many of the more CH₄-rich inclusions have compositions close to the critical curve in the system CH₄-CO₂ (Fig. 13). The lower densities of these inclusions indicate possible re-equilibration of some inclusions (Mernagh & Witt 1994, Ridley & Hagemann 1999), but there does seem to be an overall trend from denser, more CH₄-rich inclusions in veins with pyrite-pyrrhotite and pyrrhotite-albite alteration to less dense, CO₂-rich inclusions in veins with pyrite-muscovite alteration.

In contrast, the majority of liquid-rich H₂O-CH₄ inclusions show homogenization of the carbonic phase at temperatures between -87 and -84°C, which is slightly above the critical temperature of CH₄ at -82.6°C (van den Kerkhof 1988). Thus, the carbonic phase is nearly

pure CH₄, with a molar volume between 100 and 200 cm³/mole and densities around 0.92 g/cm³. These inclusions have an average temperature of homogenization of 254°C (Table 2) and are interpreted to be late, post-mineralization, secondary inclusions.

DISCUSSION

Temperature variations

Inclusions in veins with pyrite-muscovite alteration (see Table 2, Figs. 10, 11) homogenize from 98 to 316°C. These veins appear to have trapped more than one episode of fluid flow. As shown in Figure 10, there is a separate population of inclusions that homogenize below 200°C. Owing to their lower temperature of homogenization, these would seem to represent a later stage of fluid flow in these veins. Therefore, the second population of inclusions homogenizes between 210 and 316°C. This scatter in homogenization temperature is a common feature of lode-gold systems (*cf.* Ho *et al.* 1990a), and may be due to some heterogeneous trapping, post-entrapment changes, or fluctuations in pressure and temperature during fault-valve cycles in the veins (*cf.* Sibson *et al.* 1988).

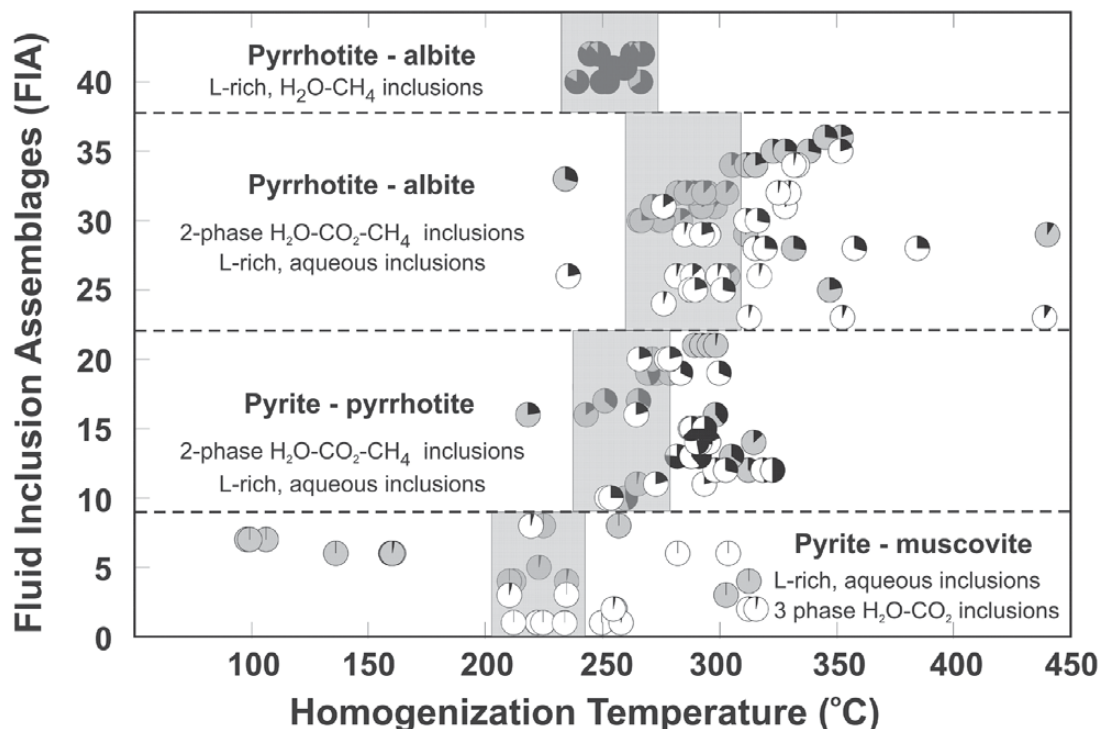


Fig. 11. A plot of temperatures of total homogenization of fluid-inclusion assemblages from each alteration assemblage. The position of the pie charts depict the homogenization temperature of the inclusions in each (FIA). Each horizontal row represents a different FIA. The black pie slice represents the mole % CH_4 in the vapor bubble, the white pie slice represents the mole % CO_2 in vapor-rich inclusions, whereas the light grey pie slice represents the mole % of CO_2 in the carbonic phase of liquid-rich, aqueous inclusions. The vol.% of H_2O in these inclusions is not shown on these pie diagrams. The secondary, liquid-rich $\text{H}_2\text{O}-\text{CH}_4$ inclusions that also occur in pyrrhotite-albite alteration are shown separately for comparison. The grey boxes depict the FIAs with the lowest temperature of homogenisation (ignoring outliers) for each alteration assemblage (see text for details).

The fluid inclusions from veins associated with pyrite-pyrrhotite alteration homogenize from 218 to 323°C (Table 2, Figs. 10, 11) and correspond well with the range of homogenization temperatures reported by Ho (1986) and Ho *et al.* (1990a). Fluid inclusions in veins associated with pyrrhotite-albite alteration homogenize from 202 to 440°C (Table 2, Figs. 10, 11). The very high temperatures of homogenization reported in this study are due to heterogeneous trapping or post-entrapment changes. Many of the inclusions display sharp edges and re-entrants on the inclusion walls, which suggests dissolution of the adjacent quartz. They closely resemble the “scalped” textures reported by Ayllón *et al.* (2003).

Temperature differences are also the simplest explanation for the contrasting alteration-induced haloes, with pyrrhotite at depth (pyrrhotite-albite haloes) and pyrite at the shallower levels (pyrite-muscovite haloes). Figure 14 illustrates how an initially H_2S -rich but sulfide-undersaturated fluid will be desulfidized by reaction

with the magnetite-rich wallrock, giving rise to the distinct zonation in a pyrrhotite-albite halo (Fig. 14a, compare Fig. 4c) at higher temperature, and in a pyrite-muscovite halo (Fig. 14b, compare Fig. 4a) at lower temperature.

A third line of evidence for temperature gradients, mainly in the lateral direction, comes from a re-interpretation of the $\delta^{18}\text{O}$ isotope data of Golding *et al.* (1990). They measured $\delta^{18}\text{O}$ in the whole rocks and the quartz veins adjacent to the Charlotte Fault, and showed that the $\delta^{18}\text{O}$ contours closely follow a fault-related indentation on the southern side of the Charlotte orebody and fault, suggesting that the strike and oblique faults were channelways for the ore fluids. High- $\delta^{18}\text{O}$ whole-rock values are coincident with the zone of sodic (pyrrhotite-albite) alteration. Golding *et al.* (1990) calculated a minimum water:rock ratio of 4 for this zone. Quartz veins near the center of the orebody have $\delta^{18}\text{O}$ values around 11‰, whereas veins around the edges of

the orebody exhibit values ranging up to 13‰. The variation in $\delta^{18}\text{O}_{\text{quartz}}$ is interpreted to be a result of a gradient in fluid temperature (Mikucki & Heinrich 1993) rather than fluid composition. Using the data on quartz–H₂O fractionation of Kawabe (1979) and assuming that the $\delta^{18}\text{O}$ of the fluid remained constant, the 2‰ range of $\delta^{18}\text{O}$ compositions in the vein quartz indicates that fluid temperatures varied over a range of 55°C. This is in general agreement with the results of the fluid-inclusion study.

Fluid-phase separation and estimates of temperature and pressure

Ramboz *et al.* (1982) have suggested three criteria for the identification of trapping of immiscible fluids: (i) the inclusions should be closely related in time and space, (ii) the inclusions should homogenize (or decrepitate) over the same range of temperature, and homogenization should be to opposite modes, (*i.e.*, to liquid and to vapor), and (iii) the relative concentration of chemical components in the liquid and vapor should be appropriate to equilibrium fractionation at total homogenization. The selection of a suitable FIA satisfies the first criterion. The coexisting liquid- and vapor-rich fluid inclusions and the overlapping temperatures of homogenization for both sets of inclusions are clearly shown in Figures 10 and 11, and the distribution of components between liquid- and vapor-rich inclusions is as expected. Textural and microthermometric data thus are consistent with trapping of immiscible fluids in the veins that generated all three types of alteration, consistent with the conclusion of Ho (1986) and Harbi (1997).

Therefore, the measured temperatures of homogenization approximate the temperatures of trapping without pressure correction, and the best estimate for the true temperature of trapping is near the lower end of the temperatures of homogenization in any one assemblage. The grey boxes in Figure 11 depict the inclusions with the lowest temperatures of homogenization (ignoring outliers) in each alteration assemblage. The temperatures of trapping indicated vary from 210 to 245°C for inclusions in veins with pyrite–muscovite alteration, from 240 to 275°C for inclusions in veins with pyrite–pyrrhotite alteration, and from 260 to 310°C for inclusions in veins with pyrrhotite–albite alteration. Figure 11 also indicates that the temperatures of trapping of inclusions increase as the alteration assemblage changes from pyrite–muscovite to pyrrhotite–albite. This result is in accord with the concentric zoning of the alteration at Mount Charlotte. Pyrrhotite–albite alteration occurs mainly within the core of the stockwork and at the deeper levels in the mine, whereas pyrite–muscovite alteration occurs in the periphery and upper levels of the orebodies (Fig. 5). Figure 11 also indicates that temperature gradients varied by up to 100°C during formation of the vein stockwork and alteration at Mount Charlotte.

Pressures are, in principle, also defined by the widespread inferred phase-separation, but an actual estimate of pressure is difficult owing to the compositionally complex CH₄–CO₂–NaCl–H₂O fluids at Mount Charlotte. The assemblage of CH₄-poor inclusions with the lowest temperature of homogenization ($T_{\text{h liquid}} \approx 210^\circ\text{C}$) and clear textural evidence of trapping in the two-phase field is FIA number 4. This assemblage contains three-phase CO₂–H₂O inclusions with $X(\text{CO}_2):X(\text{H}_2\text{O}) = 0.05$ and a bulk density of 0.974 g/cm³, estimated from the CO₂-homogenization temperature and phase-volume proportions at room temperature using the program MacFlinCor of Brown & Hagemann (1995). On the basis of experimental data for the CO₂–H₂O–NaCl solvus at 6 wt% NaCl and 4 mol.% CO₂ (Schmidt & Bodnar 2000), a fluid pressure of 600 ± 50 bar can be estimated for this assemblage. From FIAs in other parts of the vein system, significantly higher estimates of pressure are obtained, but many of those are subject to uncertainty owing to the presence of CH₄.

Methane content

There are distinct variations in the methane content of the fluids associated with each alteration assemblage. The liquid-rich H₂O–CH₄ inclusions have the most methane in the vapor phase, which contains from 66 to 100 mol.%. However, as such inclusions only occur in secondary trails in quartz veins in pyrite–muscovite and pyrrhotite–albite alteration, they are unrelated to the main phase of alteration development and will not be discussed further.

Figure 12 shows that the fluids most closely associated with pyrite–muscovite alteration contain little or no methane (≤ 2 mole % CH₄), whereas the fluids associated with pyrrhotite–albite alteration contain up to 26 mole % CH₄ in the vapor phase (Fig. 12), with bulk CO₂:CH₄ ratios ranging from ~1 to 30. Fluids associated with pyrite–pyrrhotite alteration show even larger variations in methane content, with the mole fraction of methane in the carbonic phase ranging from 0 to 1, and with the majority having values from 0.11 to 0.61 (Fig. 12).

Highly variable CO₂:CH₄ ratios are quite common in mesothermal gold-bearing fluids (Channer & Spooner 1991, Harbi 1997, Ridley & Hagemann 1999, Fan *et al.* 2000, Olivo & Williams-Jones 2002). Ridley & Hagemann (1999) attributed the variations in single veins and even within FIAs to post-entrapment re-equilibration of the inclusions. However, variation of the CO₂:CH₄ ratio due to post-entrapment changes seems unlikely in this case, as it would be expected to affect inclusions in all alteration assemblages and not just in veins with pyrite–pyrrhotite alteration. Fan *et al.* (2000) attributed the observed CO₂:CH₄ variations to either heterogeneous trapping or mixing with a reduced fluid derived from nearby graphite-bearing lithologies.

Therefore, one possibility is that CH_4 was transported into the vein network from the carbonaceous Black Flag metasediments that occur within 1 km of the Mount Charlotte deposit. Alternatively, interaction of an aqueous-carbonic fluid with partially serpentinized ultramafic lavas, occurring lower down in the stratigraphy of the Kalgoorlie region, may have generated very reduced fluids that intermittently flowed into the vein system (*cf.* Berndt *et al.* 1996).

Implications for mineralization

It is interesting that high methane contents occur most commonly in the veins associated with pyrite-pyrrhotite alteration, which constitute the most important veins in terms of bulk gold mineralization at Mount Charlotte (Fig. 5). In the ternary system $\text{CH}_4\text{-H}_2\text{O-NaCl}$, only small amounts of methane (≤ 5 mole %) are soluble in saline aqueous brines over a wide range of temperatures and pressures (up to 3 kbar and 400°C ; Naden & Shepherd 1989). Although experimental data are more limited for quaternary systems with high CO_2 contents, the presence of CH_4 in the fluid system will lead to fluid immiscibility over a wider range of temperatures and pressures. This effect may generally contribute to the formation of mesothermal lode-gold deposits over an exceptionally wide range of depths in the crust (Groves *et al.* 1992). The presence of CH_4 also may explain the formation of gold deposits in high-grade metamorphic terranes despite the progressively increasing solubility of gold at high temperatures and pressures (Mikucki 1998, Loucks & Mavrogenes 1999, Bastrakov *et al.* 2000). Phase separation driven by an influx of CH_4 into high-temperature aqueous-carbonic fluids will lead to preferential partitioning of H_2S into the vapor phase, resulting in destabilization of the gold bisulfide complex and, consequently, a reduction in gold solubility.

The fluid-inclusion data indicate that mine-scale lateral as well as vertical gradients in temperature were present during vein-stockwork formation. The shape of the zonation patterns suggests that the ore-forming fluids have cooled by as much as 100°C owing to phase separation (due to pressure fluctuations, *cf.* Drummond & Ohmoto 1985) or thermal interaction with initially colder wallrocks. Similar gradients in temperature across mineralized zones are common in shallow magmatic-hydrothermal systems, *e.g.*, porphyry copper deposits (Hedenquist *et al.* 1998), and may indicate that Mount Charlotte was formed at relatively shallow depths in the crust, consistent with the low minimum pressures estimated from fluid inclusions; these inferred pressures may indicate depths as little as 2.2 km below the surface, assuming lithostatic conditions.

Only a small amount of free gold occurs in the veins or along vein margins at Mount Charlotte (Clout *et al.* 1990). Therefore, the major phase of gold precipitation occurred as the ore-bearing fluid reacted with the host

rocks. The close spatial association between gold and the sulfide-bearing alteration haloes suggests that desulfidation of the ore-bearing fluids by reaction with wallrock Fe-silicates and carbonates was the main mechanism of gold precipitation.

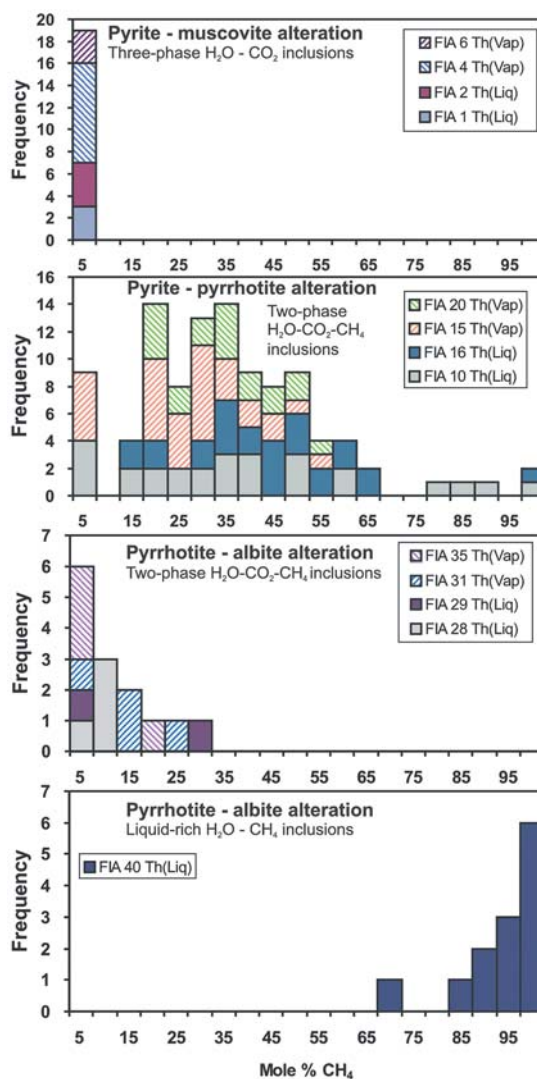


FIG. 12. Histograms showing the mole % CH_4 in the vapor phase of two- or three-phase $\text{H}_2\text{O-CO}_2(-\text{CH}_4)$ inclusions in pyrite-muscovite, pyrite-pyrrhotite, and pyrrhotite-albite alteration, as determined by laser Raman spectroscopy. The secondary liquid-rich $\text{H}_2\text{O-CH}_4$ inclusions that also occur in pyrrhotite-albite alteration are shown separately for comparison. Cross-hatched fills represent data obtained from vapor-rich inclusions, whereas solid fills depict data obtained from liquid-rich inclusions.

The tendency toward higher temperatures of mineralization for pyrite–pyrrhotite and pyrrhotite–albite alteration explains the restriction of pyrrhotite-bearing alteration assemblages to the deeper and central parts of the mine. Figure 14 shows a plot of ore–fluid evolution in redox potential (expressed as CO_2/CH_4) and H_2S activity space. Initial compositions of the fluid (marked F in the figures) are assumed to be close to the composition of the moderately reduced fluids with minor CH_4 , and a high activity of H_2S in the stability field of pyrite (but probably pyrite-undersaturated for lack of Fe), consistent with local precipitation of vein pyrite within the deepest veins associated with pyrrhotite–albite alteration (Mikucki 1998).

At temperatures around 300°C , partial desulfidation of such a hot and moderately reduced fluid owing to reaction with the wallrock will soon lead to pyrrhotite saturation (Fig. 14a), thus forming the pyrrhotite zones observed in the pyrite–pyrrhotite and pyrrhotite–albite alteration zones. The degree of reaction depends on competing reactions involving iron silicates, oxides and carbonates, but probably passes near the magnetite–pyrrhotite–pyrite triple point, as indicated by the presence of magnetite–pyrrhotite assemblages in the outer

portions of pyrrhotite–albite alteration zones. Furthermore, zoning of Fe–Ti oxide and sulfide assemblages within the alteration haloes indicates that the fluids became progressively more oxidized during reaction with the wallrocks.

At lower temperatures (*e.g.*, 225°C), the ore fluids reacting with the wallrocks became rapidly depleted in S by forming pyrite within the proximal bleached zone. At these lower temperatures, even an extremely reduced (CH_4 -dominant) fluid will not reach the stability field of pyrrhotite (Fig. 14b). Therefore, no pyrrhotite is precipitated in pyrite–muscovite alteration haloes, which follow a path of decreasing H_2S activity and increasing oxidation potential. The reaction will cease once conditions reach equilibrium with the host-rock assemblage, as indicated by R in Figure 14. Note also that gold solubility is much lower at this temperature (Fig. 14b compared with Fig. 14a), which leads to precipitation of over 99% of the gold from the fluid.

CONCLUSIONS

Fluid-inclusion data from this study indicate that temperature gradients of up to 100°C existed across the

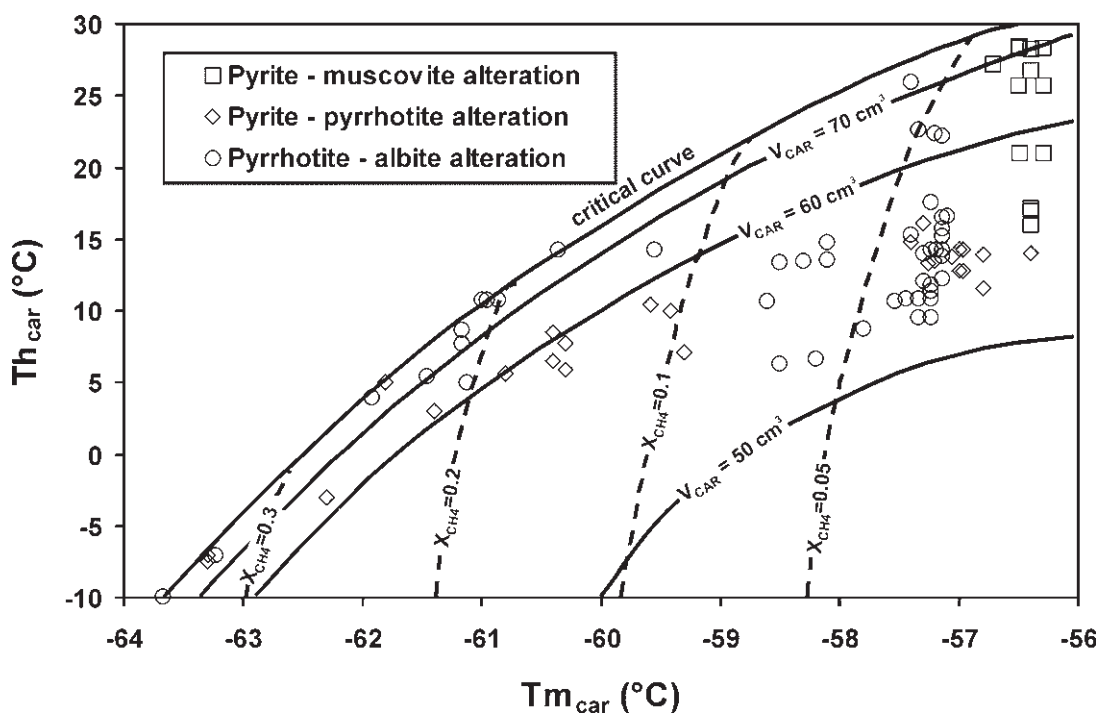


FIG. 13. Plot of homogenization temperature of the carbonic phase (T_{hcar}) versus temperatures of final melting of the carbonic phase (T_{mcar}) for $\text{H}_2\text{O}-\text{CO}_2(-\text{CH}_4)$ inclusions in the three alteration haloes. Contours of $X(\text{CH}_4)$ and V are constructed from figures in Thiery *et al.* (1994).

three alteration haloes at Mount Charlotte at the time of vein-stockwork formation, over a vertical distance of about 1 kilometer and in a lateral direction on the scale of 10–100 meters. The fluid-inclusion data indicate that the alteration zones formed over the following ranges in temperature:

Pyrite–muscovite alteration: 210 to 245°C

Pyrite–pyrrhotite alteration: 240 to 275°C

Pyrrhotite–albite alteration: 260 to 310°C

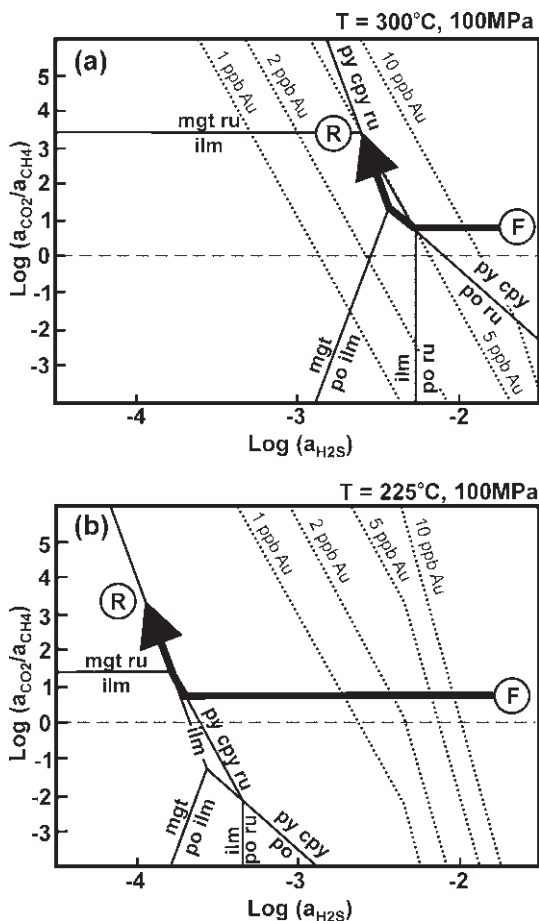


FIG. 14. Activity diagrams showing equilibrium stability relations between pyrite (Py), pyrrhotite (Po), chalcocopyrite (Ccp), magnetite (Mgt), ilmenite (Ilm) and rutile (Rt) coexisting with a C- and S-bearing aqueous fluid at (a) 300°C and (b) 225°C, and 100 MPa. The thick arrows indicate possible paths of fluid evolution at the halo scale for an ore fluid (F) progressively reacting toward equilibrium with the host rock (R). The dotted lines represent gold-solubility contours. See text for details. Thermodynamic data are based on Holland & Powell (1990), Johnson *et al.* (1992) and Turnbull & Wadsley (1986).

The chemical composition of the fluids, in terms of $\text{H}_2\text{O}:\text{CO}_2:\text{CH}_4:\text{NaCl}$, as determined by microthermometry and Raman microprobe analysis, did not vary in a systematic manner on the deposit scale, although the $\text{CH}_4:\text{CO}_2$ ratio varied over a large range. The high CH_4 contents cannot be explained by interaction with the local metagabbro wallrock, rich in magnetite \pm epidote, which takes the fluid toward increasing rather than decreasing oxidation potential. Instead, CH_4 is probably admixed from an unknown external source, such as distal carbonaceous metasediments or ultramafic lavas. Evidence for fluid-phase separation is widespread, and this process may have been driven by the widening of the two-phase stability field due to the addition of methane to an initially $\text{CO}_2\text{--H}_2\text{O}$ -dominated ore fluid. Both fluid-phase separation and lowering of the oxidation potential by incoming CH_4 will contribute to a decrease of gold solubility, and may have been initial requirements for approaching saturation in gold. The ultimate precipitation of gold together with pyrite in the alteration haloes, however, occurred by final desulfidation of the gold bisulfide complex through reaction with iron in the wallrocks. The steep vertical and lateral temperature-gradients indicate significant conductive loss of heat by a plume of hot fluid (basal input temperature possibly $>350^\circ\text{C}$) into significantly colder wallrocks (initially at $<200^\circ\text{C}$). Fluid cooling promotes the progress of the temperature-sensitive wallrock-sulfidation reactions as well as fluid-phase separation. The unusually steep temperature-gradients, caused by hot fluids focused into relatively shallow levels in the crust, are therefore the dominant cause for the exceptionally high bulk grade of gold in the Mount Charlotte deposit.

ACKNOWLEDGEMENTS

TPM publishes with the permission of the Chief Executive Officer of Geoscience Australia and Kalgoorlie Consolidated Gold Mines. We thank Evgeniy Bastrakov and Chris Heath for reviews of an earlier version of the manuscript. Gema Olivo, Philip Brown, Associate Editor Daniel J. Kontak and Robert F. Martin are thanked for their comments and suggestions, which helped improved this manuscript.

REFERENCES

- AYLLÓN, F., BAKKER, R.J. & WARR, L.N. (2003): Re-equilibration of fluid inclusions in diagenetic–anchizonal rocks of the Cinerá–Matallana coal basin (NW Spain). *Geofluids* **3**, 49–68.
- BAKKER, R.J. (1997): Clathrates: computer programs to calculate fluid inclusion V–X properties using clathrate melting temperatures. *Comput. Geosci.* **23**, 1–18.
- BASTRAKOV, E.N., CASSIDY K.F. & SHVAROV Y.V. (2000): Gold transport at Archaean lode gold deposits: gold solu-

- bility along the rock-buffered pathways. *Geol. Soc. Aust., Abstr.* **59**, 25.
- BERNDT, M.E., ALLEN, D.E. & SEYFRIED, W.E., JR. (1996): Reduction of CO₂ during serpentinization of olivine at 300°C and 500 bar. *Geology* **24**, 351-354.
- BINNS, R.A., GUNTHORPE, R.J. & GROVES, D.I. (1976): Metamorphic patterns and development of greenstone belts in the eastern Yilgarn block, Western Australia. *In The Early History Of The Earth* (B.F. Windley, ed.). Wiley, London, U.K. (303-313).
- BODNAR, R.J., BINNS, P.R. & HALL, D.L. (1989): Synthetic fluid inclusions. VI. Quantitative evaluation of the decrepitation behaviour of fluid inclusions in quartz at one atmosphere confining pressure. *J. Metamorph. Geol.* **7**, 229-242.
- _____ & VITYK, M.O. (1994): Interpretation of microthermometric data for H₂O-NaCl fluid inclusions. *In Fluid Inclusions in Minerals: Methods and Applications* (B. DeVivo & M.L. Frezzotti, eds.). Virginia Polytechnic Institute and State University Press, Blacksburg, Virginia (117-130).
- BROWN, P.E. & HAGEMANN, S.G. (1995): MacFlinCor and its application to fluids in Archaean lode-gold deposits. *Geochim. Cosmochim. Acta* **59**, 3943-3952.
- CHANNER, D.M. D. & SPOONER, E.T.C. (1991): Multiple fluid inclusion generations in variably deformed quartz: Hollinger-McIntyre and Kerr Addison-Chesterville Archaean gold-bearing quartz vein systems, northern Ontario. *Ontario Geol. Surv., Misc. Pap.* **156**, 47-64.
- CLARK, M. E. (1980): *Localization of Gold, Mt Charlotte, Kalgoorlie, Western Australia*. Honours thesis, The University of Western Australia, Perth, Australia.
- CLOUT, J.M.F., CLEGHORN, J.H. & EATON, P.C. (1990): Geology of the Kalgoorlie gold field. *In Geology of the Mineral Deposits of Australia and Papua New Guinea* (F.E. Hughes, ed.). The Australasian Institute of Mining and Metallurgy, Melbourne, Australia (411-431).
- DIAMOND, L.W. & MARSHALL, D.D. (1990): Evaluation of the fluid-inclusion crushing-stage as an aid in exploration for mesothermal gold-quartz deposits. *J. Geochem. Expl.* **38**, 285-297.
- DRUMMOND, S.E. & OHMOTO, H. (1985): Chemical evolution and mineral deposition in boiling hydrothermal systems. *Econ. Geol.* **80**, 126-147.
- DUBESSY, J., POTY, B. & RAMBOZ, C. (1989): Advances in C-O-H-N-S fluid geochemistry based on micro-Raman spectrometric analysis of fluid inclusions. *Eur. J. Mineral.* **1**, 517-534.
- FAN, HONGRUI, GROVES, D.I., MIKUCKI, E.J. & MCNAUGHTON, N.J. (2000): Contrasting fluid types at the Nevoria gold deposit in the Southern Cross greenstone belt, Western Australia: implications of auriferous fluids depositing ores within an Archaean banded iron-formation. *Econ. Geol.* **95**, 1527-1536.
- GEHRIG, M., LENTZ, H. & FRANCK, E.U. (1986): The system water-carbon dioxide-sodium chloride to 773 K and 300 MPa. *Ber. Bunsenges Phys. Chem.* **90**, 525-533.
- GOLDING, S.D., CLARK, M.E., KEELE, R.A., WILSON, A.F. & KEAYS, R.R. (1990): Geochemistry of Archaean epigenetic gold deposits in the Eastern Goldfields province, Western Australia. *In Stable Isotopes and Fluid Processes in Mineralization* (H.K. Herbert & S.E. Ho, eds.). Geology Department & University Extension, The University Of Western Australia, Perth, Australia, Publ. **23**, 141-176.
- GOLDSTEIN, R.H. & REYNOLDS, T.J. (1994): Systematics of fluid inclusions in diagenetic minerals. *SEPM (Society for Sedimentary Geology), Short Course* **31**.
- GROVES, D.I., BARLEY, M.E., BARNICOAT, A.C., CASSIDY, K.F., FARE, R.J., HAGEMANN, S.G., HO, S.E., HRONSKY, J.M.A., MIKUCKI, E.J., MUELLER, A.G., MCNAUGHTON, N.J., PERRING, C.S., RIDLEY, J.R. & VEARNCOMBE, J.R. (1992): Sub-greenschist to granulite-hosted Archaean lode-gold deposits of the Yilgarn Craton: a depositional continuum from deep-sourced hydrothermal fluids in crustal-scale plumbing systems. *In The Archaean: Terrains, Processes and Metallogeny* (J.E. Glover & S.E. Ho, eds.). Geology Department (Key Centre) & University Extension, The University of Western Australia Publication, Perth, Western Australia, 325-337.
- HARBI, H.M. (1997): *Origin of the Stockwork Gold Mineralization at Kalgoorlie, Western Australia*. Ph.D. thesis, the University of Western Australia, Perth, Western Australia.
- HEDENQUIST, J.W., ARRIBAS, A., JR. & REYNOLDS, T.J. (1998): Evolution of an intrusion-centered hydrothermal system: Far Southeast-Lepanto porphyry and epithermal Cu-Au deposits, Philippines. *Econ. Geol.* **93**, 373-404.
- HO, S. E. (1986): *A Fluid Inclusion Study of Archaean Gold Deposits in the Yilgarn Block, Western Australia*. Ph.D. thesis, the University of Western Australia, Perth, Western Australia.
- _____, BENNETT, J.M., CASSIDY, K.F., HRONSKY, J.M.A., MIKUCKI, E.J. & SANG, J.H. (1990a): Nature of ore fluid, and transportational and depositional conditions in sub-amphibolite facies deposits. *In Gold Deposits of the Archaean Yilgarn Block, Western Australia: Nature, Genesis and Exploration Guides* (S.E. Ho, D.I. Groves & J.M. Bennett, eds.). *Geology Department and University Extension, The University Of Western Australia, Perth, Western Australia, Publ.* **20**, 198-211.
- _____, GROVES, D.I. & PHILLIPS, G.N. (1990b): Fluid inclusions in quartz veins associated with Archaean gold mineralization: clues to ore fluids and ore depositional conditions and significance to exploration. *In Stable Isotopes and Fluid Processes in Mineralization* (H.K. Herbert & S.E. Ho, eds.). *Geology Department and University Extension, the University of Western Australia, Perth, Western Australia, Publ.* **23**, 35-50.

- HOLLAND, T.J.B. & POWELL, R. (1990): An enlarged and updated internally consistent thermodynamic dataset with uncertainties and correlations: the system $K_2O-Na_2O-CaO-MgO-MnO-FeO-Fe_2O_3-Al_2O_3-TiO_2-SiO_2-C-H_2O_2$. *J. Metamorph. Geol.* **8**, 89-124.
- JACOBS, G.K. & KERRICK, D.M. (1981): Methane: an equation of state with application to the ternary system $H_2O-CO_2-CH_4$. *Geochim. Cosmochim. Acta* **45**, 607-614.
- JOHNSON, J.W., OELKERS, E.H. & HELGESON, H.C. (1992): Supcr92: a software package for calculating the standard molal thermodynamic properties of minerals, gases, aqueous species, and reactions from 1 to 5000 bars and 0° to 1000°C. *Comput. Geosci.* **18**, 899-947.
- KAWABE, I. (1979): Lattice dynamical aspect of oxygen isotope partition function ratio for alpha quartz. *Geochem. J.* **13**, 57-67.
- KEATS, W. (1987): *Regional Geology of the Kalgoorlie-Boulder gold-mining district*. Geol. Surv. Western Aust., Perth, Western Australia.
- KENT, A.J.R. & MCDUGALL, I. (1995) $^{40}Ar-^{39}Ar$ and U-Pb Age constraints on the timing of gold mineralization in the Kalgoorlie gold field, Western Australia. *Econ. Geol.* **90**, 845-859.
- KERRICK, R. & FYFE, W. S. (1981): The gold-carbonate association: source of CO_2 , and CO_2 fixation reactions in Archaean lode deposits. *Chem. Geol.* **33**, 265-294.
- LIU, LIN-GUN & MERNAGH, T.P. (1990): Phase transitions and Raman spectra of calcite at high pressures and room temperature. *Am. Mineral.* **75**, 801-806.
- LOUCKS, R.R. & MAVROGENES, J.A. (1999): Gold solubility in supercritical hydrothermal brines measured in synthetic fluid inclusions. *Science* **284**, 2159-2163.
- MERNAGH, T.P. & WITT, W.K. (1994): Early, methane-rich fluids and their role in Archaean gold mineralization at the Sand King and Missouri deposits, Eastern Goldfields Province, Western Australia. *AGSO J. Aust. Geol. Geophys.* **15**, 297-312.
- MIKUCKI, E.J. (1998): Hydrothermal transport and depositional processes in Archaean lode-gold systems: a review. *Ore Geol. Rev.* **13**, 307-321.
- _____ & HEINRICH, C.A. (1993): Vein- and mine-scale wall-rock alteration and gold mineralization in the Archaean Mount Charlotte deposit, Kalgoorlie, Western Australia. In Kal '93, Kalgoorlie, 1993. *Aust. Geol. Surv. Organisation Record*, 135-140.
- _____ & RIDLEY, J.R. (1993): The hydrothermal fluid of Archaean lode-gold deposits at different metamorphic grades: compositional constraints from ore and wallrock alteration assemblages. *Mineral. Deposita* **28**, 469-481.
- NADEN, J. & SHEPHERD, T.J. (1989): Role of methane and carbon dioxide in gold deposition. *Nature* **342**, 793-795.
- NEALL, F.B. & PHILLIPS, G.N. (1987): Fluid-wallrock interaction in an Archaean hydrothermal gold deposit: a thermodynamic model for the Hunt mine, Kambalda. *Econ. Geol.* **82**, 1679-1694.
- OLIVO, G.R. & WILLIAMS-JONES, A.E. (2002): Genesis of the auriferous C quartz-tourmaline vein of the Siscoe mine, Val d'Or District, Abitibi Subprovince, Canada: structural, mineralogical and fluid inclusion constraints. *Econ. Geol.* **97**, 929-947.
- PASTERIS, J.D., WOPENKA, B. & SEITZ, J.C. (1988): Practical aspects of quantitative laser Raman microprobe spectroscopy for the study of fluid inclusions. *Geochim. Cosmochim. Acta* **52**, 979-988.
- PECHER, A. (1981): Experimental decrepitation and re-equilibration of fluid inclusions in synthetic quartz. *Tectonophysics* **78**, 567-583.
- PHILLIPS, G.N. & GROVES, D.I. (1983): The nature of Archaean gold-bearing fluids as deduced from gold deposits of Western Australia. *J. Geol. Soc. Aust.* **30**, 25-39.
- RAMBOZ, C., PICHAVANT, M. & WEISBROD, A. (1982): Fluid immiscibility in natural processes: use and misuse of fluid inclusion data. *Chem. Geol.* **37**, 29-48.
- RIDLEY, J.R. & DIAMOND, L.W. (2000): Fluid chemistry of orogenic lode gold deposits and implications for genetic models. *Rev. Econ. Geol.* **13**, 141-162.
- _____, GROVES, D.I. & MIKUCKI, E.J. (1994): Major Archaean lode-gold deposits: fluid focussing and chemical evolution in vertically extensive hydrothermal systems. *Geol. Soc. Aust., Abstr.* **37**, 374.
- _____ & HAGEMANN, S.G. (1999): Interpretation of post-entrapment fluid-inclusion re-equilibration at the Three Mile Hill, Marvel Loch and Griffins Find high-temperature lode-gold deposits, Yilgarn Craton, Western Australia. *Chem. Geol.* **154**, 257-278.
- _____ & MENGLER, F. (2000): Lithological and structural controls on the form and setting of vein stockwork orebodies at the Mount Charlotte gold deposit, Kalgoorlie. *Econ. Geol.* **95**, 85-98.
- ROBERT, F. & KELLY, W.C. (1987): Ore-forming fluids in Archean gold-bearing quartz veins at the Sigma mine, Abitibi greenstone belt, Quebec, Canada. *Econ. Geol.* **82**, 1464-1482.
- ROEDDER, E. (1984): Fluid Inclusions. *Rev. Mineral.* **12**.
- SCHMIDT, C. & BODNAR, R.J. (2000): Synthetic fluid inclusions. XVI. PVTX properties in the system $H_2O-NaCl-CO_2$ at elevated temperatures, pressures, and salinities. *Geochim. Cosmochim. Acta* **64**, 3853-3869.
- SCOTT, R.J. (1997): Fault control on fluid flow and mineralization at Mount Charlotte and the Golden Mile. *Aust. Geol. Surv. Organisation Rec.* **1997/41**, 145-150.

- SIBSON, R.H., ROBERT, F. & POULSON, K.H. (1988): High-angle reverse faults, fluid pressure cycling and mesothermal gold-quartz deposits. *Geology* **16**, 551-555.
- SWAGER, C., GRIFFIN, T.J., WITT, W.K., WYCHE, S., AHMAT, A.L., HUNTER, W.M. & MCGOLDRICK, P.J. (1990): Geology of the Archaean Kalgoorlie terrain – an explanatory note. *Geol. Surv. Western Australia, Rec.* **1990/12**.
- THIERY, R., VAN DEN KERKOF, A.M. & DUBESSY, J. (1994): V_x properties of CH_4 - CO_2 and CO_2 - N_2 fluid inclusions: modelling for $T < 31^\circ\text{C}$ and $P < 400$ bars. *Eur. J. Mineral.* **6**, 753-771.
- TRAVIS, G.A., WOODALL, R. & BARTRAM, G.D. (1971): The geology of the Kalgoorlie goldfield. *Geol. Soc. Aust., Spec. Publ.* **3**, 175-190.
- TOURET, J.L.R. (2001): Fluids in metamorphic rocks. *Lithos* **55**, 1-25.
- TURNBULL, A.G. & WADSLEY, M.W. (1986): *The CSIRO-SGTE Thermodata System, Version V*. CSIRO Division of Mineral Chemistry Communication, Melbourne, Australia **7**.
- VAN DEN KERKOF, A.M. (1988): *The System CO_2 - CH_4 - N_2 in Fluid Inclusions: Theoretical Modelling and Geological Applications*. Ph.D. thesis, Vrije Universiteit, Amsterdam, The Netherlands.
- WITT, W. K. (1991): Regional metamorphic controls on alteration associated with gold mineralization in the Eastern Goldfields province, Western Australia: implications for the timing and origin of Archean lode-gold deposits. *Geology* **19**, 982-985
- WOODALL, R.W. (1965): Structure of the Kalgoorlie goldfield. *In Geology of Australian Ore Deposits* (J. McAndrew, ed.). The Australasian Institute of Mining and Metallurgy, Melbourne, Australia (71-79).
- YEATS, C.J. & VANDERHOR, F. (1998): Archean lode-gold deposits. *AGSO J. Aust. Geol. Geophys.* **17**, 253-258.

Received November 8, 2002, revised manuscript accepted May 13, 2003.